Fig S1. Theory results for yielding behaviour in an unbounded Hele-Shaw extensional flow. A) Coordinate system. B) Contours of $\phi \left(\frac{J}{m^3-s} \right)$ are plotted in $X-Y$ plane, where $X, Y \in (-3d, 3d)$ and $Z = d/20$, which is assumed to be very close to the midplane. The rheological parameters of 0.3% CS were used: $\tau_y = 1.29$ Pa and $\mu \approx 2.49$ Pa $-$ s. An experimental G ($\approx 0.055 \, s^{-1}$) is calculated at $\Delta P = 241$ kPa for 0.3% CS. The contour of ϕ_y is denoted by a dotted circle. The region within this circle is unyielded. This analysis is compared with the experimental S, as denoted by a solid line depicting a square. The size of these two regions is of the same order. However, if we choose a different Z for the calculation (for example, $Z = d/100$) of ϕ, the size of the dotted region will change. Therefore, we should limit these calculations to the comparison of the order of magnitudes. C) Contours of ϕ are plotted in $X-Z$ plane, where $Z \in (0, d/2]$. The rest of the parameters stay the same. The contour of ϕ_y is denoted by a dotted curve. The size of the unyielded region grows from the top plane as we approach the midplane, and diverges at $Z = 0$. However, we do not see this diverging effect in both simulation and experiments and are likely be a feature of an 'unbounded' flow. D) Theoretical S estimated by calculating $G \approx U_{at \, M}/D_{M-O}$ for several ΔP using ϕ_y and $Z = d/20$ vs. the experimental S for 0.3% CS. Here, we should limit the comparison to order of magnitude, which appears to be satisfied.
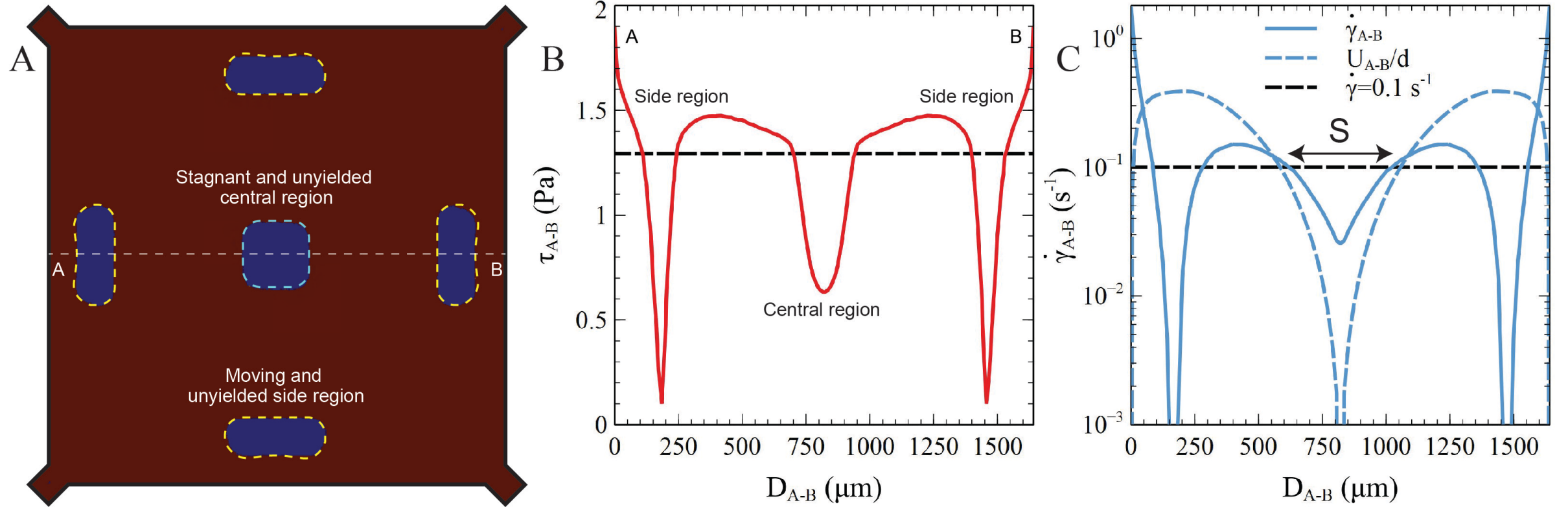
Fig S2. Simulation results for 0.3% CS. A) Unyielded zones at $\Delta P / \tau_y W d^2 \mathcal{R}_o = 0.015$ is shown using the definition of yielding zone used in COMSOL. We observe that at the midplane, the shape of the unyielded zone at the stagnation point is not circular as predicted by the theory. But it is roughly square in shape, similar to the square channel. This is in agreement with the experiments. Moreover, we also observe four additional unyielded regions near each of the four walls of the channel. These are the regions where the fluid enters, moves like a plug, and then leaves. Fluid in these regions is not stagnant. We do not observe these side regions in our experiments. Thus, we do not take them into consideration while calculating the yield stress. The differences in the theory and simulation could be arising due to the four falls bounding the flow and providing no-slip surfaces. B) The shear stress, τ_{A-B}, vs. D_{A-B}. τ_{A-B} is higher near the wall, dips down as we move away from the wall, again increases and peaks, and further drops down closer to the stagnation point. We also show the yield stress line for comparison. In both the side and central regions, $\tau_{A-B} < \tau_y$, exhibiting unyielding. C) A comparison of strain rate along $A - B$ using the definition $\dot{\gamma} \equiv \sqrt{\frac{1}{2} \dot{\gamma}_{ij} \dot{\gamma}_{ji}}$ and $\dot{\gamma} \sim U/d$. Both are of the same order closer to the center, and thus, the region below $\dot{\gamma} = 0.1 \text{ s}^{-1}$ is roughly of the same size for both. Thus, the strain rate scale we used for the detection of the unyielded region is a reasonable assumption.
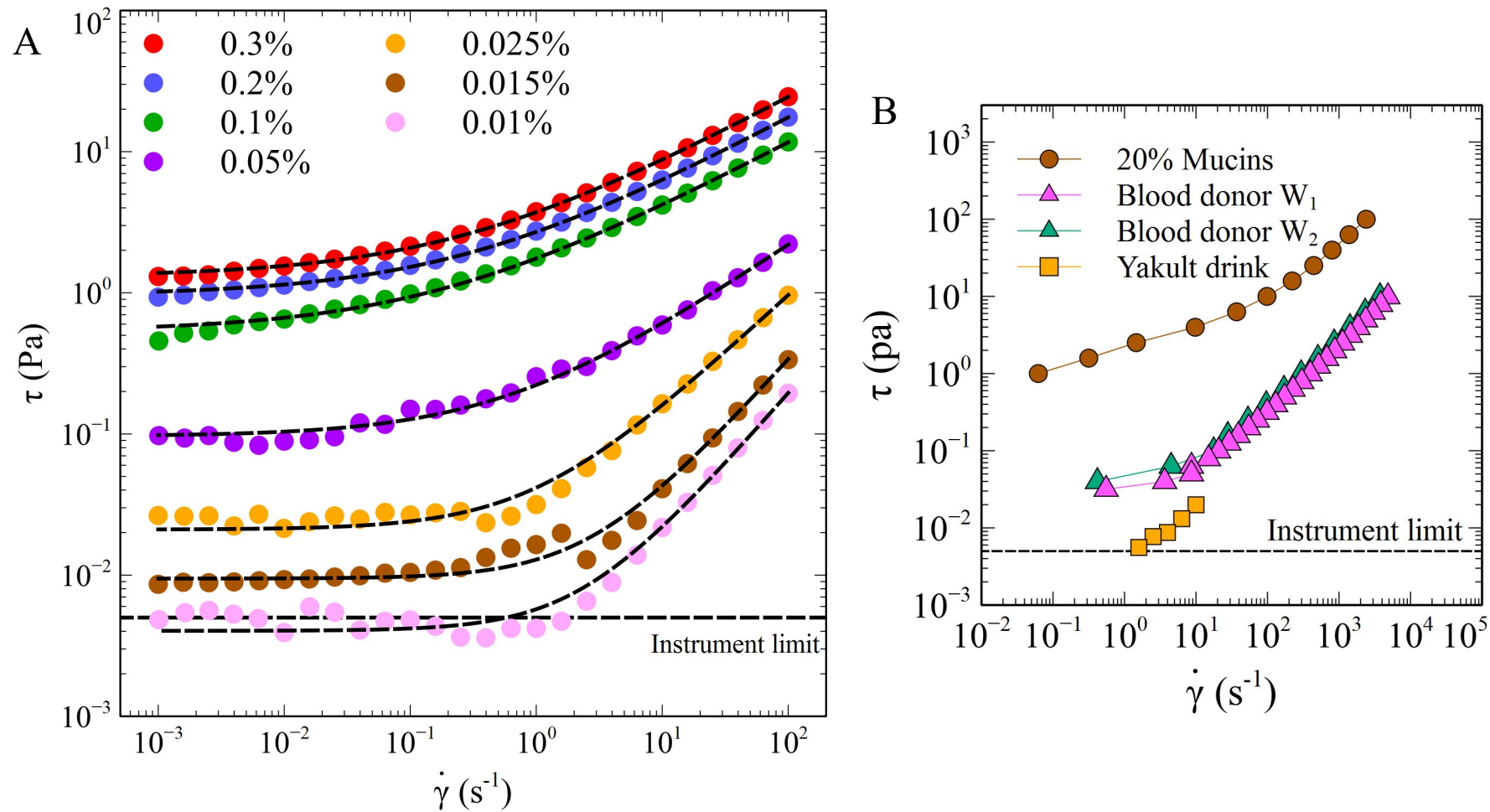
Fig S3. Rheological measurements: A) Shear stress, τ (Pa), vs. shear rate, $\dot{\gamma}$ (s^{-1}), measured for Carbopol of a range of concentrations between 0.010 to 0.3%. The dotted lines demonstrate Herschel-Bulkley fits and the Herschel-Bulkley parameters are listed in ESI Table S1. Further, we also show the instrument limit by a horizontal dotted line, which is determined by reference oils and water as shown in Fig.S4. Here, the data for 0.01% CS coincides with the instrument limit. For lower concentrations, τ for $\dot{\gamma} < 1\,s^{-1}$ plateaus around the same limit. Consequently, we exclude concentrations lower than 0.015% from our calculations. We performed multiple runs of the rheological tests and are reporting the ones which do not have any erratic data points or missing data points. B) τ (Pa) vs. $\dot{\gamma}$ (s^{-1}) of whole blood obtained from two female donors, W_1 and W_2, 20% mucin suspensions, and Yakult® lactic drink. Details about rheology are presented in Materials and methods in the main text.
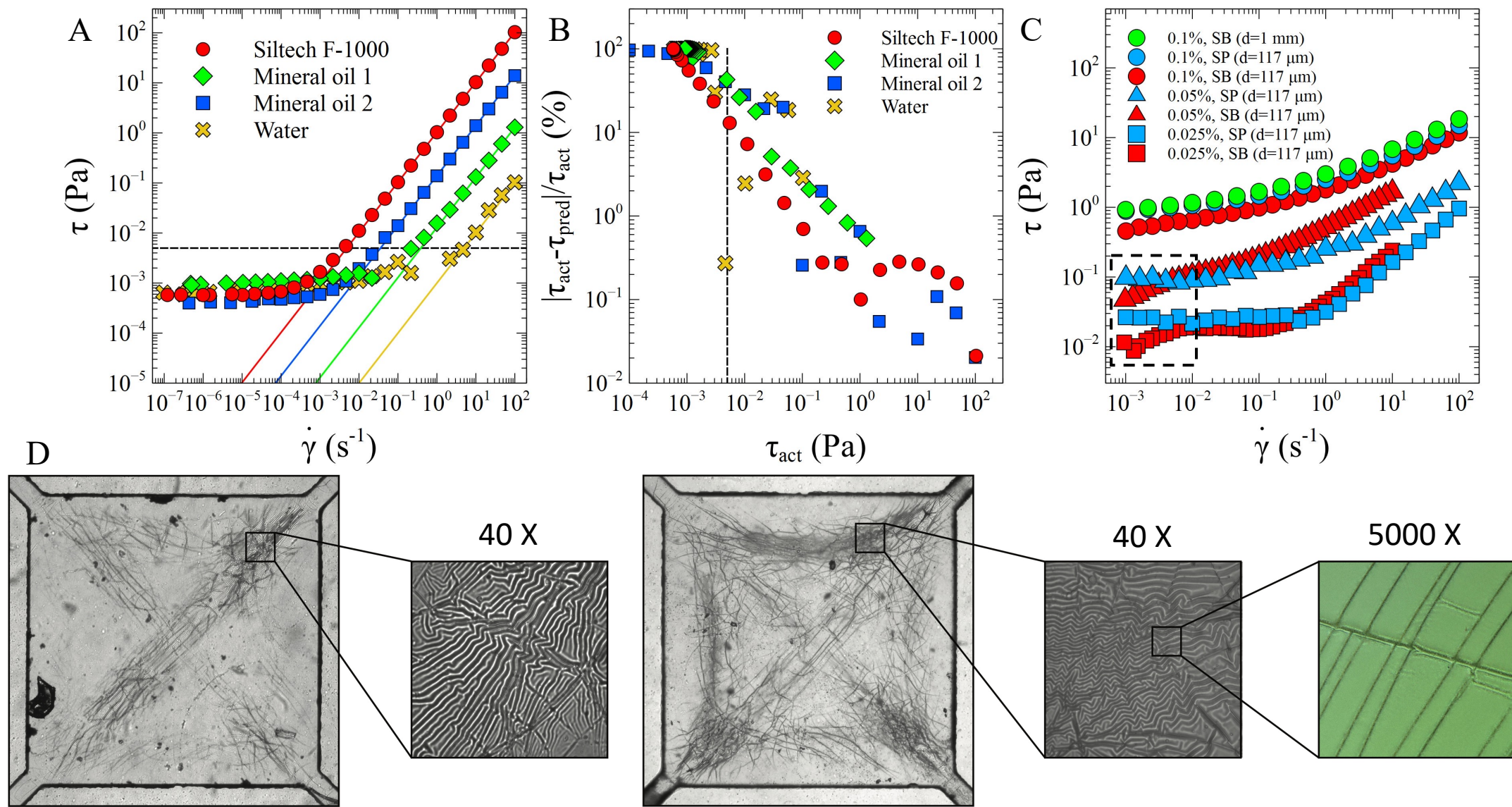
Fig S4. Limitations: A) τ (Pa), vs. $\dot{\gamma}$ (s^{-1}), measured for four reference fluids 1) reference oil (Siltech F-1000), 2) light mineral oil (Mineral oil 1), 3) white mineral oil (Mineral oil 2), and water. Here, we varied $\dot{\gamma}$ between $10^2 - 10^{-7} s^{-1}$. The solid lines represent the Newtonian τ for the given $\dot{\gamma}$. We observe that for each of the four fluids, there is a deviation of τ from the Newtonian τ when τ was close to ≈ 5 mPa (dotted line), and finally it plateaus when $\tau \sim O(1)$ mPa. B) The error between actual τ and Newtonian or predicted τ is given by $|\tau_{act} - \tau_{pred}|/\tau_{act}$ vs. τ_{act}. We observe a significant error of 10%, when $\tau_{act} \approx 5$ mPa. C) τ (Pa), vs. $\dot{\gamma}$ (s^{-1}) measured for three samples (0.025,0.05, and 0.1%) with different gap size between the parallel plates of the rheometer ($d = 117$ µm or 1 mm) and different wall conditions (1. SB: sandblasted top and smooth bottom plate or 2. SP: sandpaper on both sides). D) Two examples of our used microfluidic devices. We can see streaks of roughness introduced during plasma treatment process. The pictures on the sides are captured using 40X lens. We also show one example of roughness with 5000X lens. We observe that roughness is of the order of 1 µm in size.

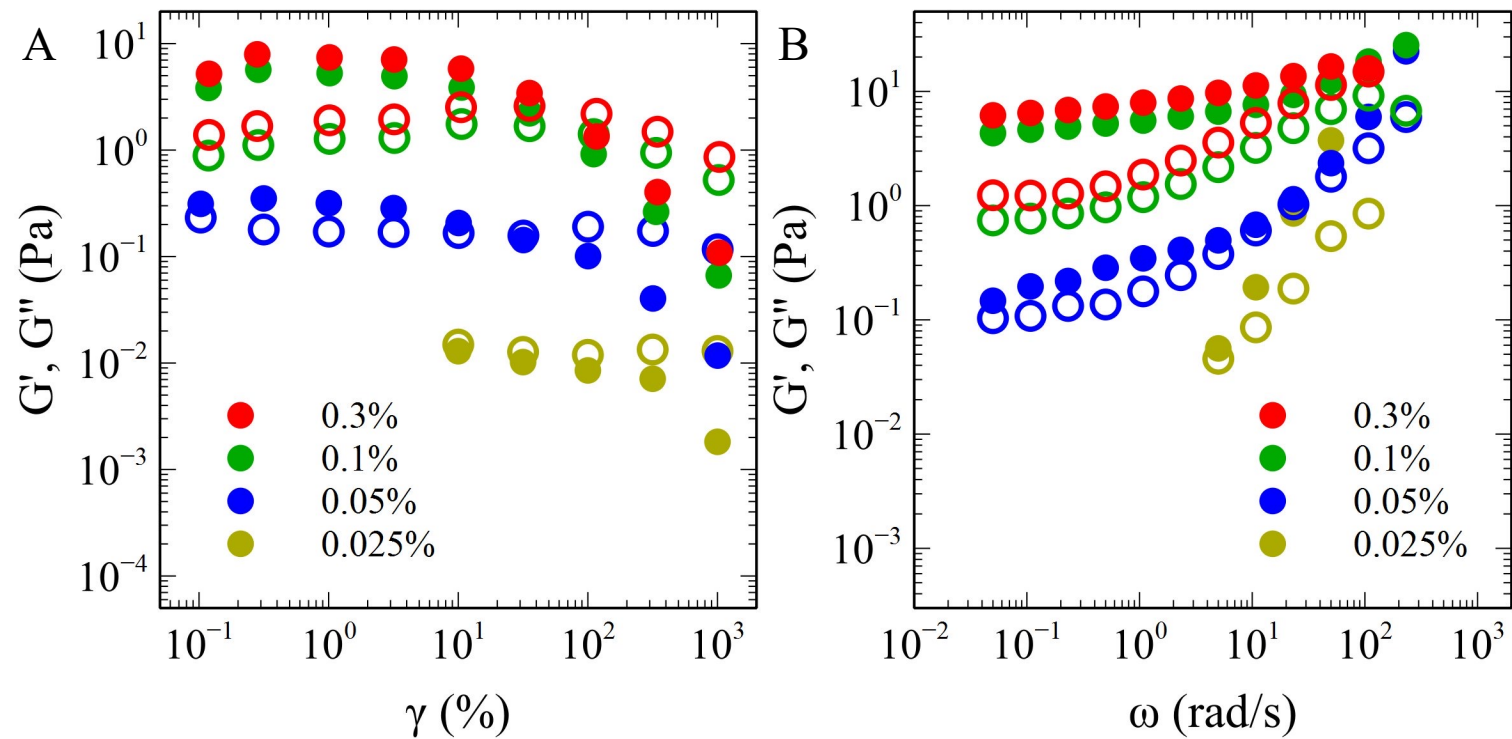**Fig S5.** Oscillatory rheology. A) Large amplitude oscillatory study. Storage modulus, G', and loss modulus, G'', vs. strain $\gamma(\%)$ for four samples (0.025 − 0.3% CS) at frequency (ω) of 1 rad/s. B) Small amplitude oscillatory study. G', G'', vs. ω at $\gamma = 1\%$.
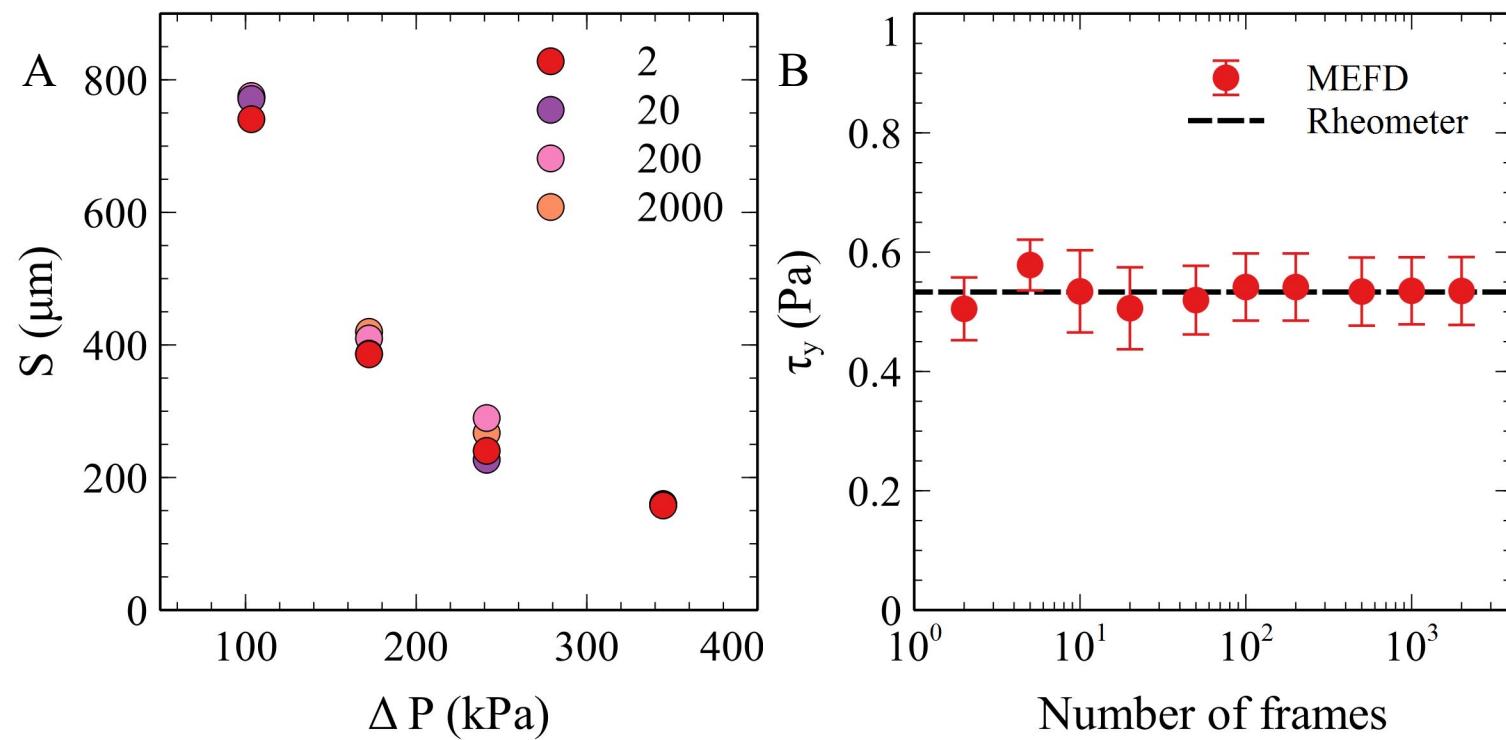
Fig S6. Measurement of yield stress for various time scales. A) S vs. ΔP for 0.1% CS at different number of images used for analysis. B) τ_y vs. number of frames analyzed. We recorded a long video (30 fps) for a few minutes for 0.1% CS at a range of ΔP, and used different number of images for analysis. For example, if we consider 100 images, then we pick first 100 images, and calculate the velocity field averaging over these 100 images to calculate S, and measure τ_y using Eqn. 5. The rheometer τ_y is shown for comparison.
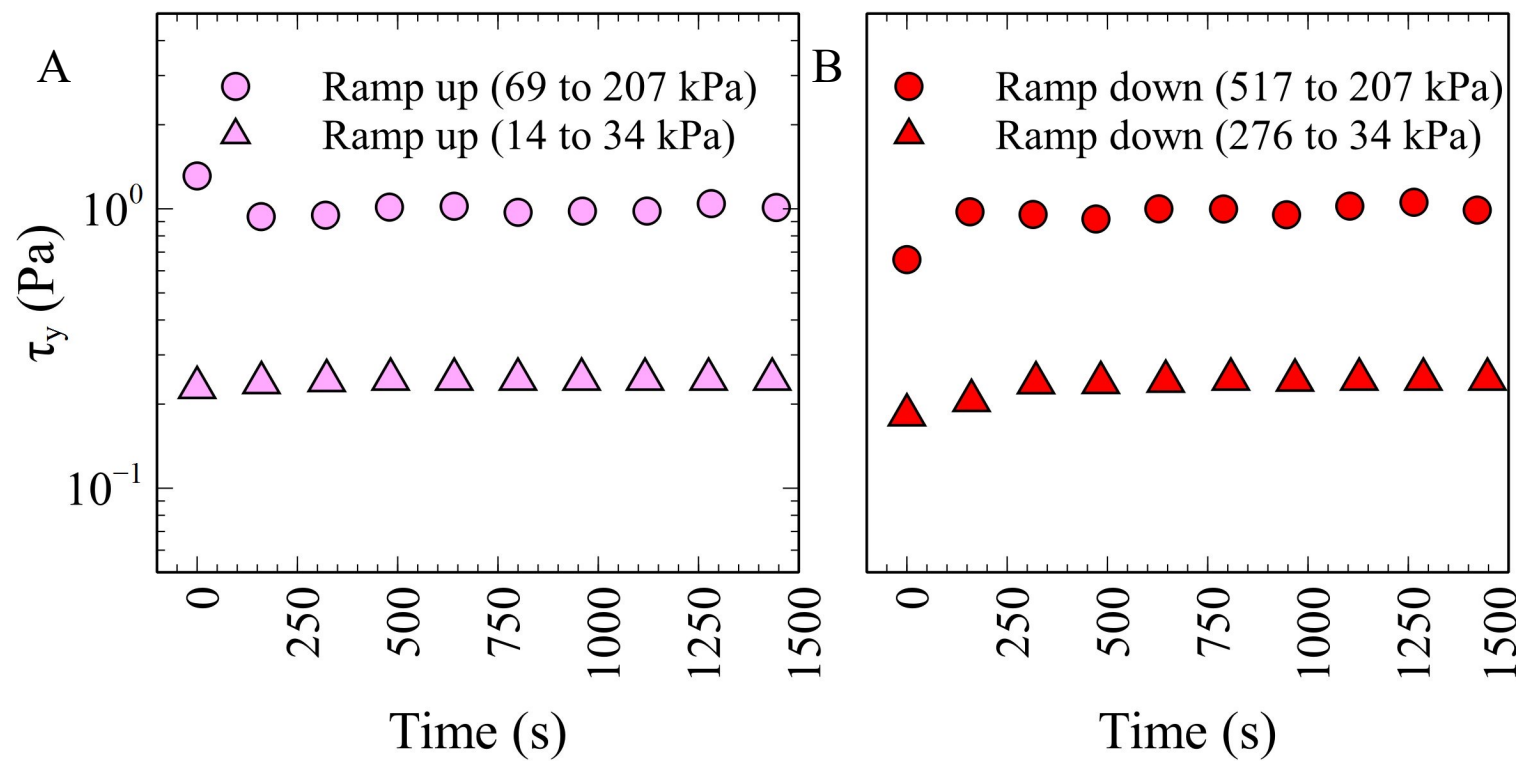
Fig S7. Pressure ramps using real-time measurement of τ_y using 100 images for analysis. A) Ramp up: τ_y vs. Time (s) for 0.3 and 0.05% CS shown by circle and triangle, respectively. τ_y was measured right after ΔP was ramped up (values of ΔP are provided in the bracket). B) Ramp down: τ_y vs. Time (s) for 0.3 and 0.05% CS. In each case, since we begin the measurements post-ramp up or ramp down, we observe a small bump in the beginning.
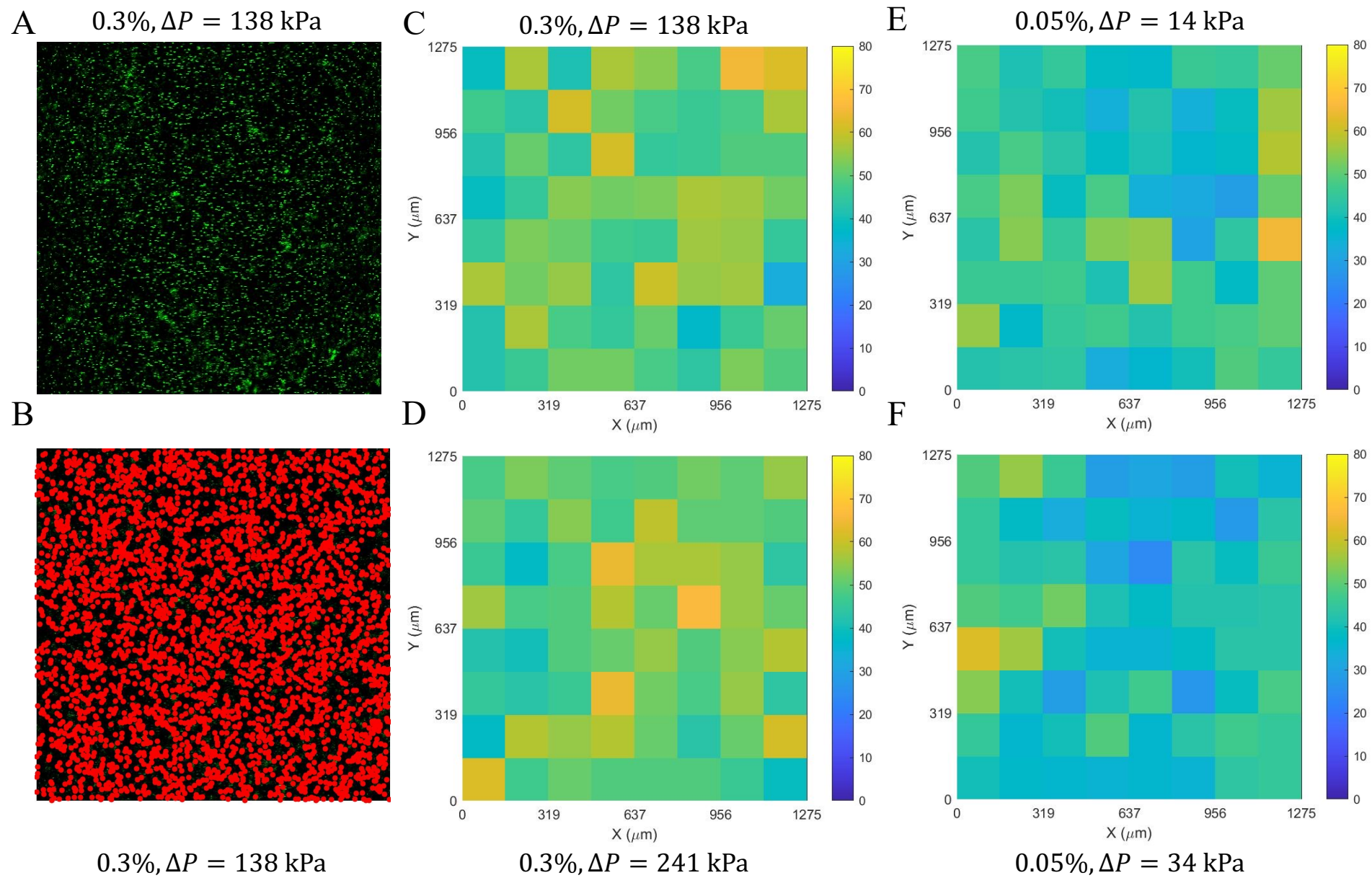
Fig S8. Particle density measurements. A) A snapshot from the experimental video of 0.3% CS at $\Delta P = 138$ kPa. B) Tracked particles from the image in A. C) The density of particles is presented by dividing the image into a grid of 8×8 for the figure B. The colourbar shows particle density. Figure D E and F depict the density of particles measured for 0.3% at higher $\Delta P = 241$ kPa, 0.05% at higher $\Delta P = 14$ kPa, and 0.05% at higher $\Delta P = 34$ kPa, respectively.
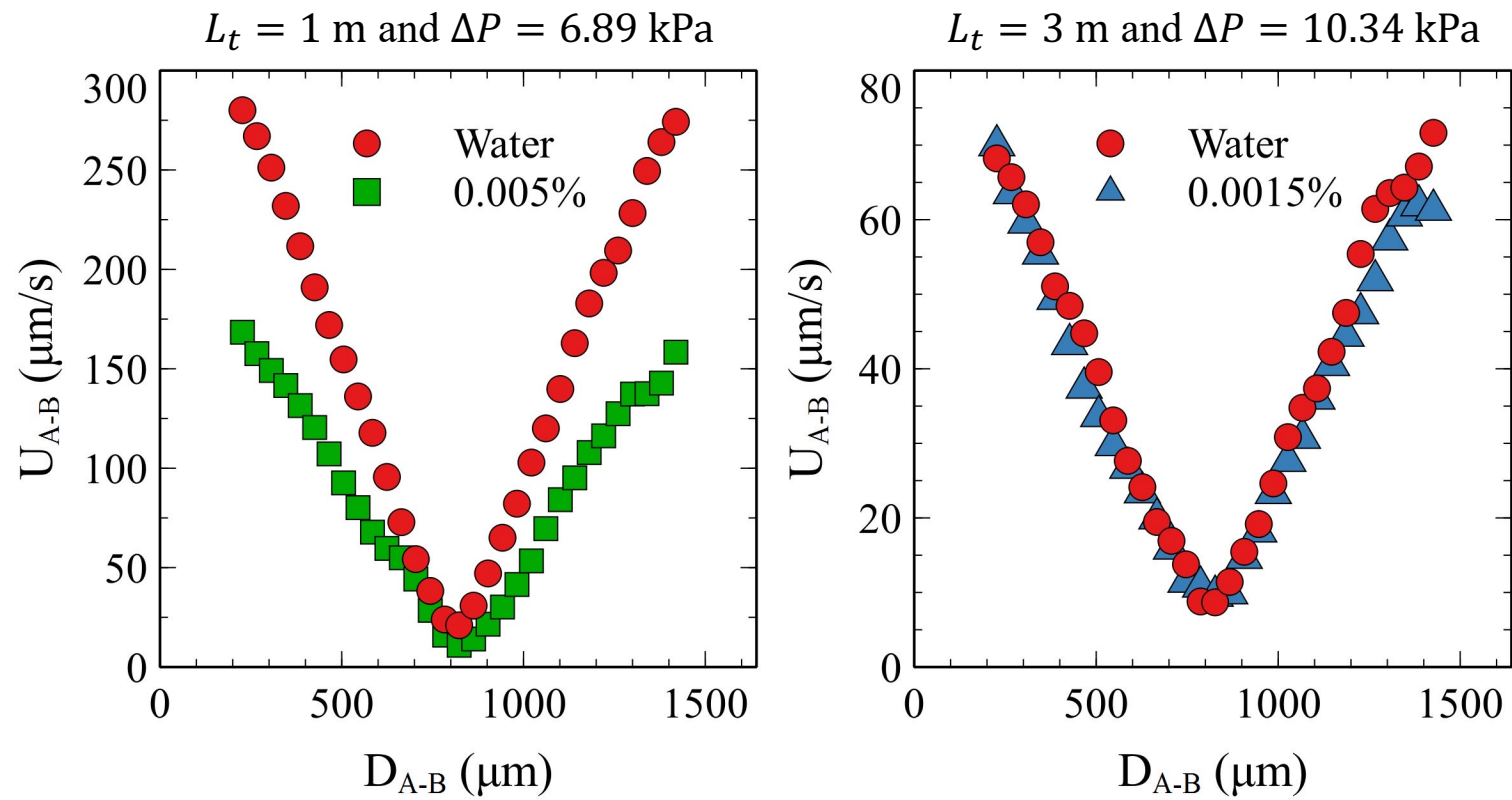
Fig S9. Velocity comparison. A) Comparison of U_{A-B} vs. D_{A-B} for water and 0.005% CS. B) Comparison of U_{A-B} vs. D_{A-B} for water and 0.0015% CS. Further details about length of the PEEK tube and pressure drop are provided in the figures.
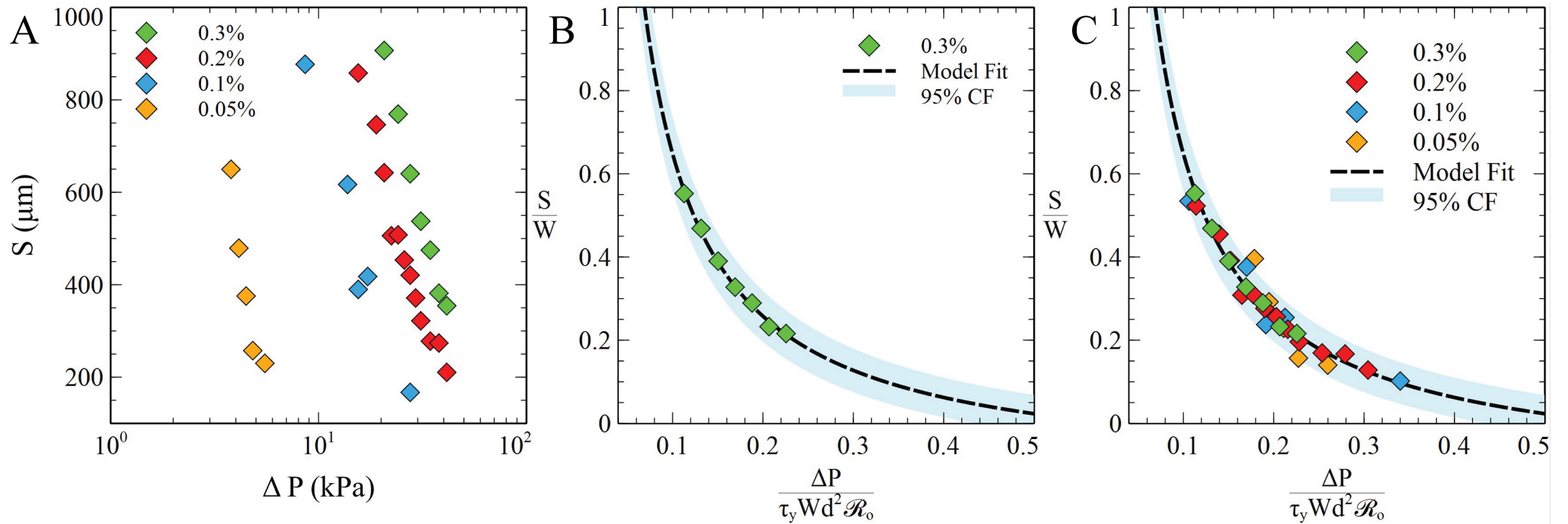
Fig S10. Experimental results for the tube of $d_t = 508$ μm. A) S (μm) vs. ΔP (kPa) for CS of concentration, C_{CS}, between 0.05 to 0.3%. B) Dimensionless data, S/W and $\Delta P/\tau_y W d^2 \mathcal{R}_o$, is represented ($\tau_y = \tau_{yR}$) for 0.3% CS. This data is fitted to Eqn. 4 to obtain the characterization curve, or the model fit as shown in the figure. C) S/W vs. $\Delta P/\tau_y W d^2 \mathcal{R}_o$ ($\tau_y = \tau_{yM}$) is plotted for CS of a range of C_{CS} (0.05 to 0.3%). 95% confidence interval for the model fit is shown by the blue shaded region.
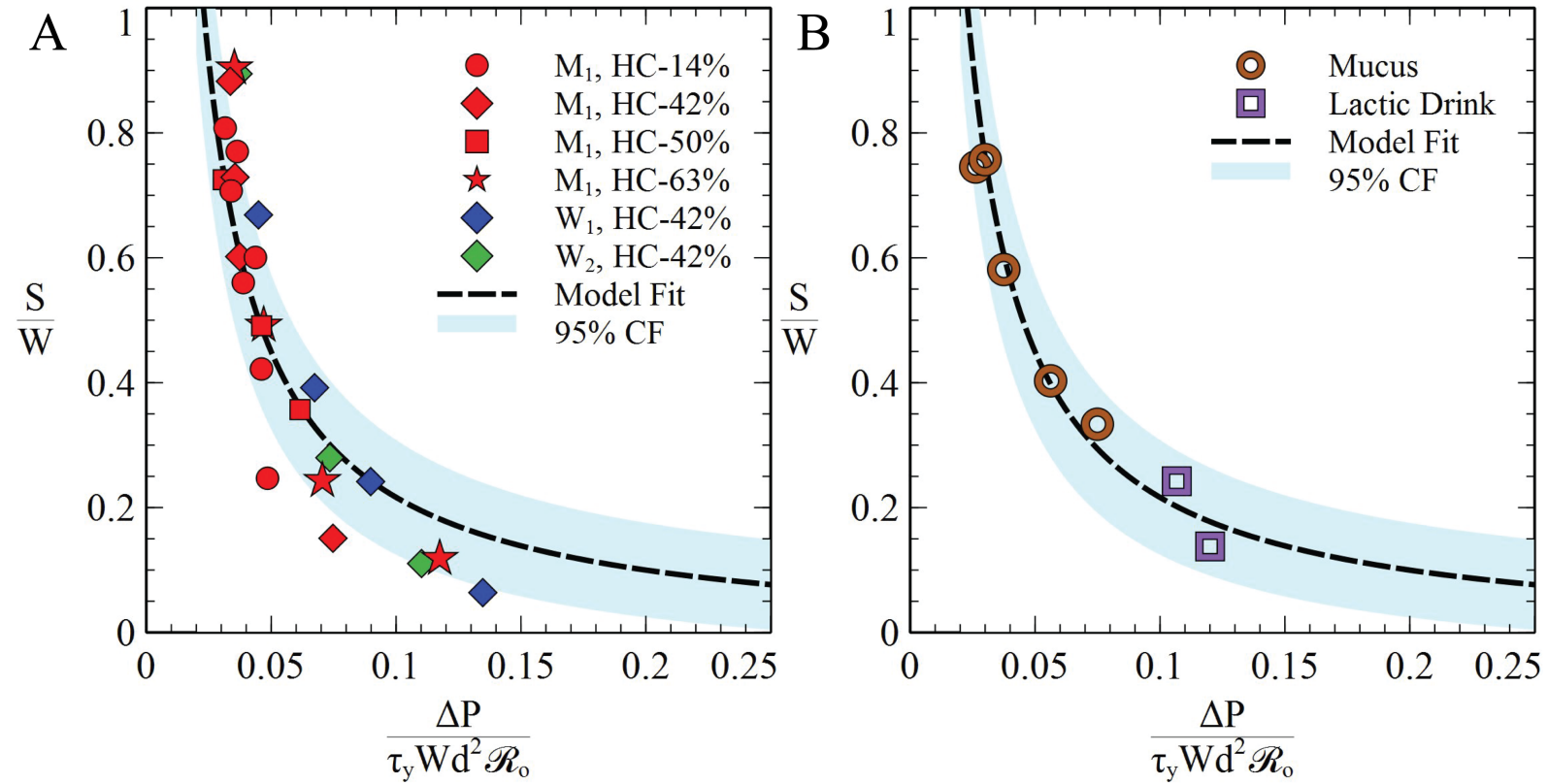
Fig S11. Experimental results for blood, 20% mucin suspension (denoted as mucus in the plot), and Yakult® lactic drink. A) S/W vs. $\Delta P/\tau_y W d^2 \mathcal{R}_o$ ($\tau_y = \tau_{yM}$) is plotted for various blood samples obtained from three donors $M_1, W_1,$ and W_2 of physiological hematocrit ($HC \approx 42\%$). M_1 sample is further reconstituted to obtain HC of $14, 50,$ and 63%. B)) S/W vs. $\Delta P/\tau_y W d^2 \mathcal{R}_o$ ($\tau_y = \tau_{yM}$) is plotted for 20% mucins and lactic drink. 95% confidence interval for the model fit is shown for both by the blue shaded region.
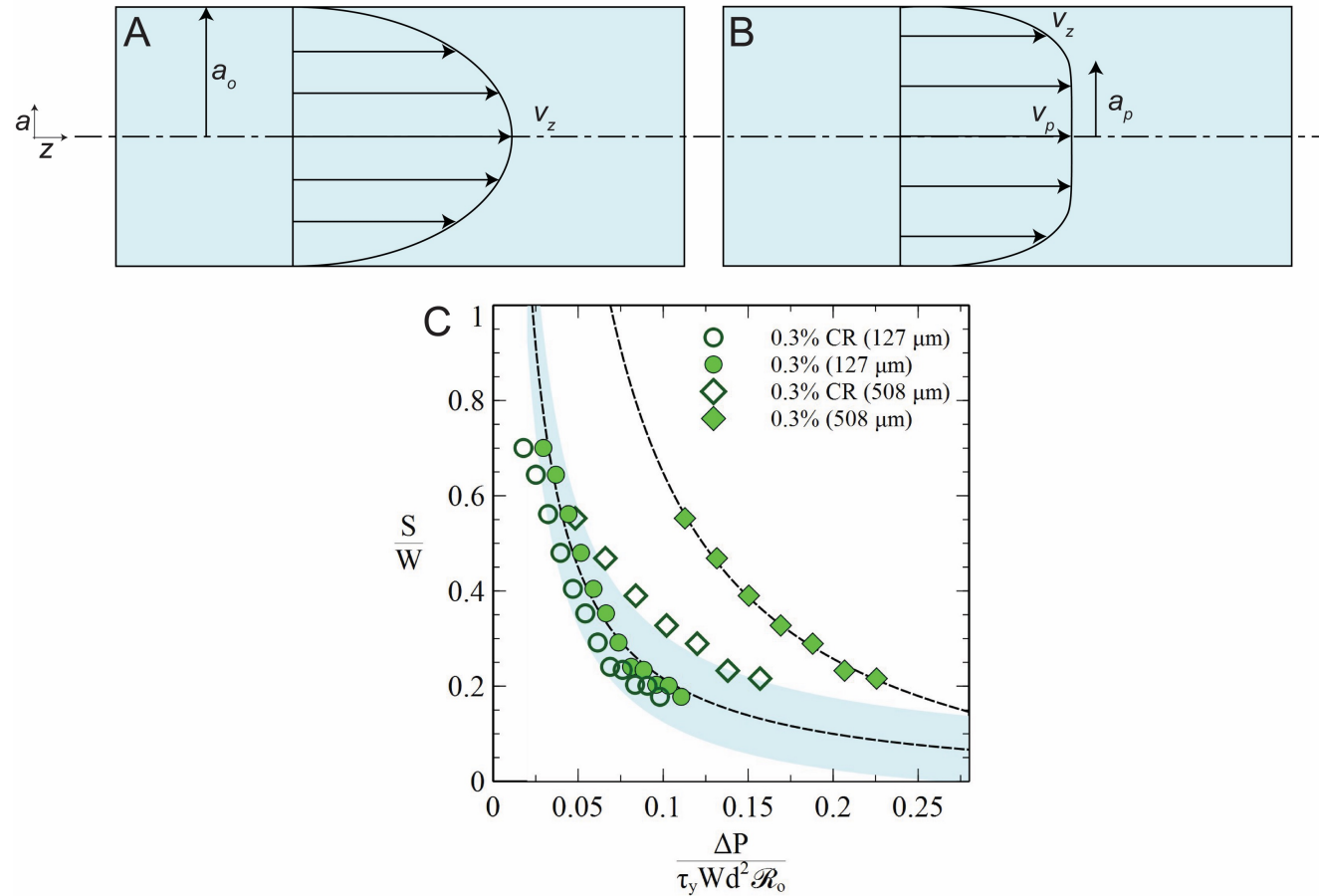
Fig S12. Correction to the flow resistance using the Bingham plastic model. A) Flow of Newtonian fluid through a tube of radius, a_o, with a velocity v_z along the z direction. B) Flow of Bingham fluid through a tube. The unyielding leads to the formation of plug at the center of radius, a_p, moving at a constant velocity, v_p. In both cases, v_z is a function of (a, z). C) The scaled data, S/W and $\Delta P/\tau_y W d^2 \mathcal{R}_{oN}$, for 0.3% CS in both the tubes and the respective model fits are shown by the filled symbols and dotted line, respectively, where $\mathcal{R}_{oN}$ is the flow resistance for a Newtonian case. Empty symbols show the data $\Delta P/\tau_y W d^2 \mathcal{R}_{oBP}$, calculated using the corrected resistance (CR) for a Bingham Plastic fluid, $\mathcal{R}_{oBP}$. In the case of $d_t = 127$ μm, the shift in the corrected scaled data is minimal and it lies within the confidence interval for the most part. For the larger tube ($d_t = 508$ μm), the shift in the corrected scaled data is significant, and is almost falling into the confidence interval of the 127 μm case.
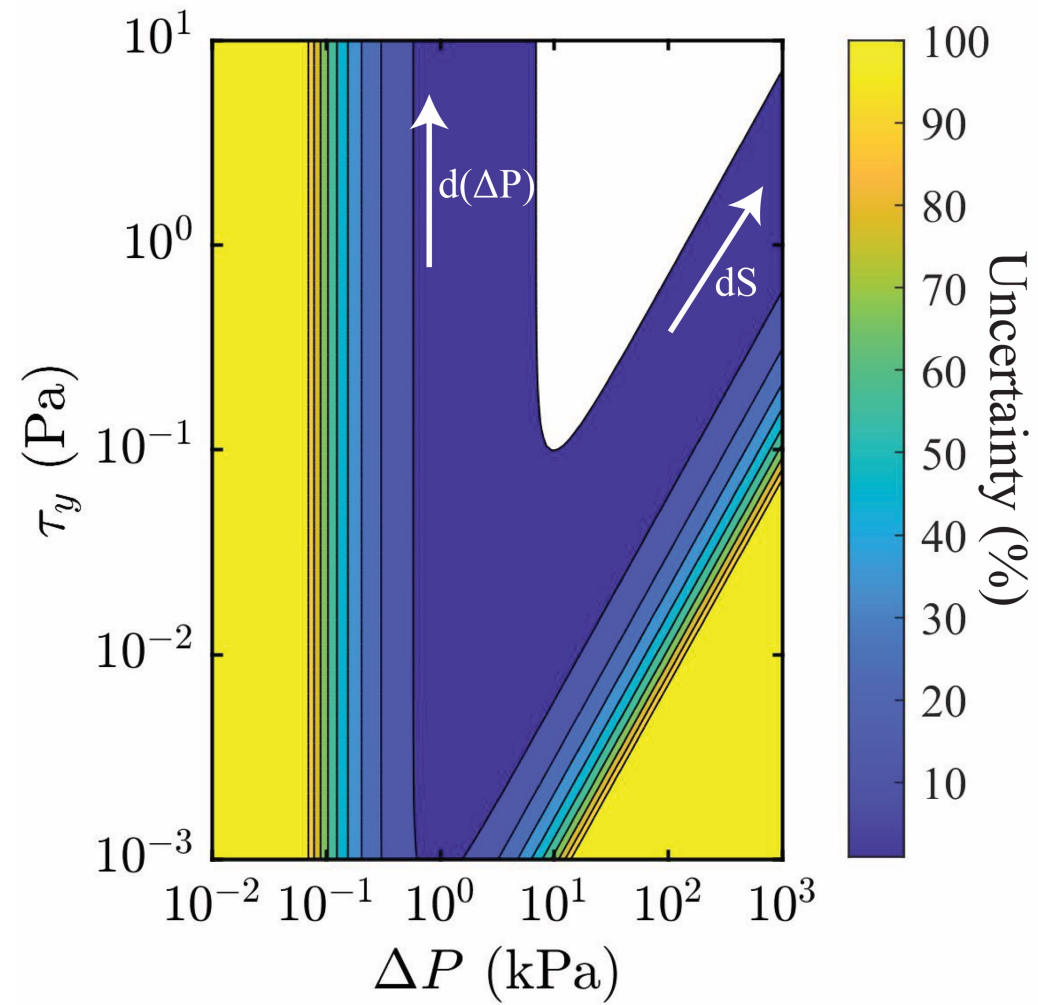
Fig S13. Contours of uncertainty (%) calculated for different sets of τ_y and ΔP for $d_t = 127$ μm. A colourbar is shown on the right depicting the uncertainty in the measurement of τ_{yM} using the MEFD technique.
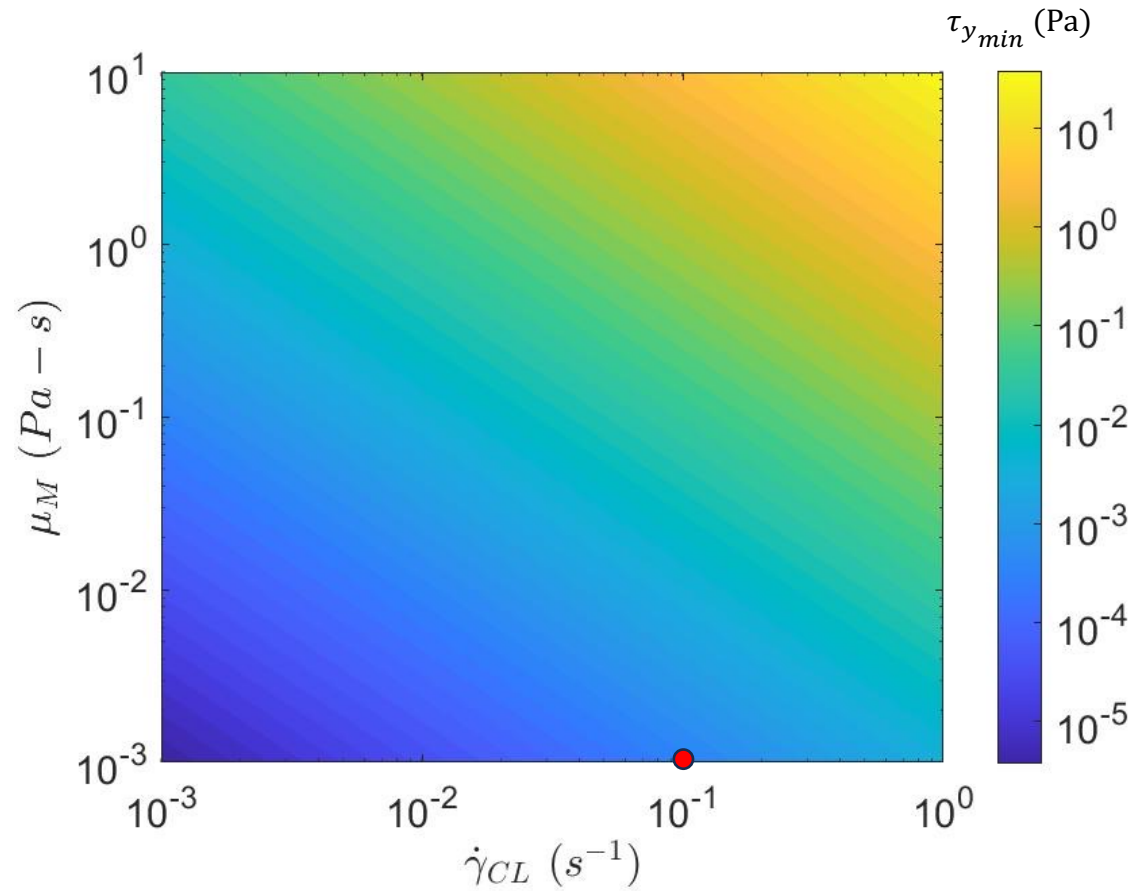
Fig S14. Contours of $\tau_{y\,min}$ (Pa) as a function of viscosity, μ_M (Pa − s), of suspending medium of a suspension and the strain rate criterion, $\dot{\gamma}_{CL}$ (s^{-1}). The colourbar represents $\tau_{y\,min}$ (Pa). The red dot represents the conditions used in this study, where our suspensions are water based ($\mu_M = 10^{-3}$ Pa − s) and strain rate criterion ($\dot{\gamma}_{CL} = 10^{-1}$ s^{-1}).